Theory of fiber optic radiometry, emissivity of fibers, and distributed thermal sensors

Albert Zur and Abraham Katzir

This paper formulates a general radiometric theory of multimode step index fibers, covering in particular the region of mid- and far IR fibers. The optical fiber is treated both as a passive waveguide, guiding the external radiation injected into it, as well as an active waveguide, generating internal thermal radiation which is guided to both fiber endfaces. Several fiber absorption profiles are considered. In other words, the thermal radiation sources coupling radiation into the guided modes of the fiber are in one case considered to be distributed in the core, and in another, to be distributed in the cladding. The model is based on 3-D optical geometry of bounded and tunneling skew rays and yields an analytical expression for the angular power distribution along the length of the fiber. The radiation emissivity of multimode fibers is formulated. Based on the model, the theory of a new fiber optic distributed thermal sensor is presented. This sensor needs no external source of radiation for its operation and is based on the self-generation of thermal radiation in a modified IR fiber. Such a sensor can be produced by deliberately inducing surface or bulk absorption in the fiber core or coating (cladding) a bare fiber core with an IR absorbing material.

I. Introduction

A number of publications have described the use of IR fibers in radiometric thermometry.[1–6] In these papers the optical fiber is used as a flexible waveguide to deliver radiation from a thermal source (not necessarily in direct line of sight) to an IR detector. The radiation power allows one to determine the object's temperature. This mode of operation is called point thermal sensing. In a previous paper, we propose another operation mode in which an IR multimode fiber is used as a new type of fiber optic distributed thermal sensor (FDTS), requiring no external source of radiation for its operation.[7] This sensor can be produced by deliberately inducing absorption in the core or cladding of an IR fiber. The absorption profile of the modified fiber determines the sensing length of the FDTS. When a fiber element along the sensing length is heated, this induces the self-emission of thermal radiation in the fiber. Part of this radiation is coupled into guided modes and transmitted in the same fiber to both its endfaces. The measurement of this radiation makes it possible, with what we term a first-order sensor, to determine the average spatial temperature distributed along the fiber's sensing length. With another sensor, which we term a second-order sensor, the location of a hot spot can also be determined. These sensors can be installed along flexible paths in volume spaces and have a potential application in distributed thermal sensing, such as the thermometry of cavities, calorimetry, fluid level sensing, overheating and hot spot detection, heat conductivity measurements, and so on. Thermal sensing is possible by contact, by conduction, or by convection and radiation (noncontact).

Progress has recently been made in the subfield of IR fibers. There has been an increase in the amount of work published on IR fiber radiometry. However, no complete theoretical formulation of this subject exists in the literature. We were therefore motivated in this paper to formulate a radiometric theory of multimode IR fibers. The model is based on 3-D optical geometry of bounded and tunneling skew rays, and Kirchhoff's law of radiation absorption–emission. The model considers not only the radiation penetrating the fiber endfaces from the outside, but also the thermal radiation generated within the fiber from sources (fiber absorption) located in the core and in the cladding. The successive Fresnel reflection at both fiber endfaces are also considered. The problem of power coupling into guided modes from sources uniformly distributed in the cladding has been discussed by Marcuse.[8] However, his formulation does not take into account the attenuation of radiation by the same

The authors are with Tel Aviv University, School of Physics & Astronomy, Tel Aviv 69978, Israel.

Received 20 March 1990.
0003-6935/91/060660-14$05.00/0.

sources in the cladding and thus predicts that the guided power coupled into the fiber will increase linearly with fiber length. This might be correct if the sources are fluorescent. However, when the sources are thermal, this prediction violates the conservation of energy, since one can obtain a sufficiently long fiber where the endface emission exceeds that of a blackbody. It would appear that the framework of the formulation presented below, which is based on geometric optics and Kirchhoff's law, provides a simple adequate solution to the problem of thermal radiation sources located both in the cladding and in the core. The model yields an analytical expression for the angular power distribution guided along the length of the fiber to both its endfaces.

The following topics are discussed in the body of the paper. Section II discusses general fiber optic radiometry, A 3-D model of bounded and tunneling skew rays which takes into account the generation, transmission, and attenuation of radiation in the fiber. Section III deals with the emissivity of multimode fibers. Thermal radiation emission from the fiber endfaces is formulated and compared to that of a blackbody. Section IV discusses the fiber optic distributed thermal sensor (FDTS), a model considering three basic profiles of fiber absorption yielding the distributed sensing. Sources of thermal radiation associated with fiber absorption are considered in the core surface, in the core bulk, and in the cladding. The model inherently predicts the optimal sensor parameters yielding maximum sensitivity for each absorption profiles of the FDTS.

II. General Fiber Optic Radiometry

Let us consider an ideal multimode fiber with a step index, not restricted to weak guidance, for which the V-number $[\equiv (2\pi a/\lambda)(n_{co}^2 - n_{cl}^2)^{1/2}]$ is much higher than unity. Such fibers are best suited for thermal radiometry. Since thermal sources are diffuse and incoherent, ray optics is a good approach for considering these fibers, providing an intuitive and fairly accurate analytical solution compared to the modal approach. Our purpose is to determine the angular distribution of the radiation power guided along the fiber by bounded and tunneling skew rays. We consider two sources of guided radiation: external radiation coupled into the fiber at the endfaces, and internal thermal radiation generated in the core and in the cladding. In general, the fiber interacts thermally with the environment by conduction, convection, and radiation and can be a source or a sink of heat. Let us consider a short fiber element Δx of uniform steady state temperature T, located at a distance x from fiber endface 1 (see Fig. 1). The spectral power emitted from this element is distributed across the invariant guiding parameters of a ray in the fiber, angles θ and γ; θ is the inclination angle between the ray's path and the axis of the fiber, while γ is the skewness angle between the projection of the ray's path on the fiber cross section and the fiber's radius. The power distribution emitted from this element can be written in the form

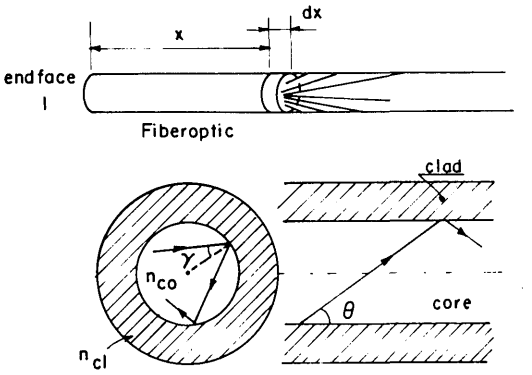

Fig. 1. Thermal radiation emission from fiber element dx. Inclination angle θ and skewness angle γ of a guided ray are illustrated.

$$P_\lambda(x + \Delta x,\theta,\gamma) = P_{bb\lambda}[T(x),\theta,\gamma]\epsilon_\lambda(\Delta x) + P_\lambda(x,\theta,\gamma)\exp[-\alpha_t(\theta,\gamma,\lambda)\Delta x]. \quad (1)$$

The first term represents the guided part of the thermal radiation generated from a fiber element having a cross-sectional area πa^2 (where a is the fiber's radius). This radiation emission is represented by that of a blackbody $P_{bb\lambda}$ with corresponding sensitivity $\epsilon_\lambda(\Delta x)$ and is formulated in Appendix A as Eq. (A5), giving

$$P_{bb\lambda}[T(x),\theta,\gamma] = 8a^2 W_{bb\lambda}[T(x)]\cos\theta\sin\theta f(\gamma,\theta), \quad (1a)$$

where

$$W_{bb\lambda}(T) = \frac{c_1}{\lambda^5}\left[\exp\left(\frac{c_2}{\lambda T}\right) - 1\right]^{-1},$$

$$c_1 = 37413\,\frac{W\mu^4}{\mathrm{cm}^2}, \quad c_2 = 14{,}388\,\mu\mathrm{K}.$$

The skewness distribution function $f(\gamma,\theta)$ is defined in Eq. (A5a). This function describes how the power emitted from a blackbody fiber element at an inclination angle θ is distributed across the various skew angles γ. The spectral emissivity $\epsilon_\lambda(\Delta x)$ of the fiber element Δx combines all the mechanisms of radiation generation in the fiber. Using Kirchhoff's law, the emissivity can be written as

$$\epsilon_\lambda(\Delta x) = 1 - \exp[-\alpha_{ab}(x,\theta,\gamma,\lambda)\Delta x]. \quad (1b)$$

$\alpha_{a,b}$, the effective modal absorption coefficient of the fiber, is formulated in Appendix B. Equation (1b) implies that a better absorber is a better emitter. Any power absorption mechanism of the guided modes is also a source of thermal radiation coupled into the same guided modes. Absorption in the fiber core is one source, and absorption in the cladding (evanescent waves) is another. This principle considerably simplifies the procedure. It eliminates the need to calculate coefficients for the power coupling of each thermal radiation source in the fiber to the guided modes—a cumbersome calculation, particularly for multimode fibers. The principles underlying modal fiber absorption are dealt with in Appendix B.

The second term in Eq. (1) represents the power transmitted through the fiber element, part of which is

lost due to absorption and scattering in the fiber. This loss of power is represented by the total (extinction) attenuation coefficient of the fiber, which is written as the sum of two terms: absorption and scattering

$$\alpha_t(x,\theta,\gamma,\lambda) = \alpha_{ab}(x,\theta,\gamma,\lambda) + \alpha_{sc}(x,\theta,\gamma,\lambda). \quad (2)$$

Both terms are considered to be dependent on the longitudinal coordinate x and are formulated in Appendix B. Where Δx becomes a differential dx, Eq. (1) yields the following differential equation:

$$\frac{\partial P_\lambda(x,\theta,\gamma)}{\partial x} = 8a^2 W_{bb\lambda}[T(x)]\alpha_{ab}(x,\theta,\gamma,\lambda) \times \cos\theta \sin\theta f(\gamma,\theta) - \alpha_t(x,\theta,\gamma,\lambda)P_\lambda. \quad (3)$$

This equation governs the physics underlying fiber optic radiometry. The general solution of this equation is

$$P(x) = P_{in}\exp[-\alpha(x)] + g\exp[-\alpha(x)]\int_0^x W_\lambda[T(x')]\exp[\alpha(x')]dx', \quad (4)$$

where new definitions are introduced, shortening the notation by omitting the obvious dependence on θ, γ, and λ:

$$g \equiv 8a^2\cos\theta\sin\theta f(\gamma,\theta),$$
$$W_\lambda[T(x')] \equiv \alpha_{ab}(x',\theta,\gamma,\lambda)W_{bb\lambda}[T(x)], \quad (4a)$$
$$\alpha(x) \equiv \int_0^x \alpha_t(x',\theta,\gamma,\lambda)dx'.$$

If the fiber attenuation coefficient α_t is uniform along the length of the fiber, $\alpha(x)$ is reduced to $\alpha_t(\theta,\gamma,\lambda)x$. The first term in Eq. (4) is determined by the boundary condition $P_{in} \equiv P_\lambda(x = 0,\theta,\gamma)$, i.e., by the power distribution (in the core medium) at the fiber input face. Equation (4) shows that the power carried in the fiber has two sources: external radiation penetrating the fiber at the input face (first term) and internal thermal radiation generated within the fiber (second term). Each fiber element dx emits blackbody radiation with emissivity of $\alpha_{ab}dx$. This radiation is guided through the fiber to the output face with a loss of $\exp[-\alpha_t(L - x)]$, where L is the fiber's length. The distributed thermal sensor[7] is based on this property.

The next step in this formulation is to include the successive Fresnel reflections at the fiber endfaces. These reflections alter the power distribution of Eq. (4), particularly in the higher modes which involve stronger reflections. This is used in Sec. IV for the purpose of enhancing sensor efficiency by heightening the reflection from one of the fiber endfaces. For unpolarized ($\perp$,$\parallel$) thermal radiation, the reflection factor at each fiber endface is

$$r = \tfrac{1}{2}[r_\perp(\theta,\lambda) + r_\parallel(\theta,\lambda)], \quad (5)$$

where $r_\perp$ and $r_\parallel$ are the known Fresnel reflection factors for the two polarization states. These are determined by the angle of incidence θ (irrespective of the skewness angle γ), and by n_{co} and $n_{1,2}$, which are the refractive indices of the core and of the medium outside the fiber at the faces, respectively. We introduce this Fresnel factor to solve the generation–transmission problem and include in this discussion the contribution to input and output of both fiber endfaces. Consider an input power p_{in1} coupled into fiber face 1, and p_{in2} into face 2. Our purpose is to determine output power P_{out2} from the fiber endface 2 and P_{out1} from endface 1, taking into account all the successive reflections back and fourth of the radiation guided in the fiber (see Fig. 2). Formally, this can be written as

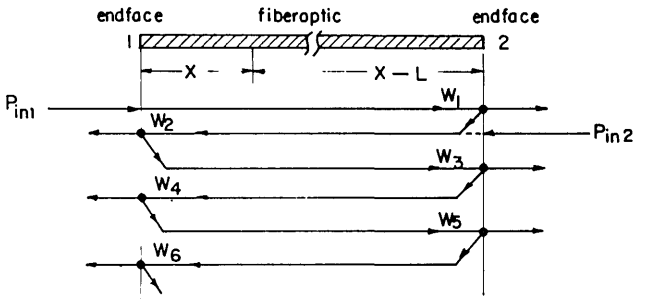

Fig. 2. Diagram of successive reflections at the fiber endfaces by which the power distribution in the fiber was calculated.

$$P_{out2} = (W_1 + W_3 + W_5 + \ldots)(1 - r_2),$$
$$P_{out1} = (W_2 + W_4 + W_6 + \ldots)(1 - r_1). \quad (6)$$

The term W_i is the output power (in the core medium) from reflection number $(i - 1)$. r_2 and $(1 - r_2)$ are, respectively, the reflection and transmission factors at fiber endface 2. By analogy, r_1 and $(1 - r_1)$ are the same factors for endface 1 (r_1 and r_2 are not generally equal). The term W_1 is the power transmitted to endface 2 from endface 1 and from the emitting medium along the length of the fiber. It is derived from Eq. (4) as follows:

$$W_1 = g\exp[-\alpha(L)]\int_0^L W_\lambda[T(x)]\exp[\alpha(x)dx] + (1 - r_1)P_{in1}\exp[-\alpha(L)], \quad (6a)$$

where L is the fiber's length. To obtain W_2, we again use Eq. (4), but this time in the coordinate system $x - L$ rather than x. P_{in} now includes two terms: the reflected part of W_1 and the transmitted part of P_{in2} at fiber endface 2. Thus,

$$W_2 = g\int_0^L W_\lambda[T(x)]\exp[-\alpha(x)]dx + [r_2W_1 + (1 - r_2)P_{in2}]\exp[-\alpha(L)]. \quad (6b)$$

As can be seen from W_1 and W_2, the blackbody radiation generated in the fiber is guided through it in two directions, to endface 1 and to endface 2. All the other terms in Eq. (6) are calculated by tracing the successive reflections and by introducing the losses due to endface reflections and fiber attenuation. We thus obtain

$$W_3 = r_1W_2\exp[-\alpha(L)], \quad W_4 = r_2W_3\exp[-\alpha(L)],$$
$$W_5 = r_1W_4\exp[-\alpha(L)], \quad W_6 = r_2W_5\exp[-\alpha(L)], \quad (6d)$$

Substituting Eq. (6a) and all odd terms of Eq. (6c) into Eq. (6) gives the total output power emerging from fiber endface 2:

$$P_{out2} = g\int_0^L W_\lambda[T(x)]\{\exp[-\alpha(L)]R_{ev2}\exp[\alpha(x)] + R_{od2}\exp[-\alpha(x)]\}dx + (1-r_1)R_{ev2} \times \exp[-\alpha(L)]P_{in1} + (1-r_2)R_{od2}\exp[-\alpha(L)]P_{in2}, \quad (7)$$

where the multireflection factors R_{ev} and R_{od} are defined as follows:

$$R_{ev2}(\theta,\gamma,\lambda) = \frac{1-r_2}{1-r_1r_2\exp[-2\alpha(L)]},$$
$$R_{od2}(\theta,\gamma,\lambda) = \frac{(1-r_2)r_1\exp[-\alpha(L)]}{1-r_1r_2\exp[-2\alpha(L)]}. \quad (7a)$$

If $r_1 = r_2 = 0$ (when $n_{1,2} = n_{co}$), $R_{od} = 0$ and $R_{ev} = 1$, and Eq. (7) is reduced to Eq. (6a), that is, $P_{out2} = W_1$. The new (second) term in braces in Eq. (7) originates from the successive reflections of the guided radiance at the fiber endfaces. This term implies that the greater a fiber element's distance from output endface 2 (the lower x), the lower will be the transmission loss of the blackbody radiation emitted from this fiber element, contradicting the first term in the braces which has already appeared in Eq. (6a). Substituting Eq. (6b) and all even terms of Eq. (6c) into Eq. (6) gives the total output power emerging from fiber endface 1:

$$P_{out1} = g\int_0^L W_\lambda[T(x)]\{\exp[-\alpha(L)]R_{od1}\exp[\alpha(x)] + R_{ev1}\exp[-\alpha(x)]\}dx + (1-r_1)R_{od1}\exp[-\alpha(L)]P_{in1} + (1-r_2)R_{ev1}\exp[-\alpha(L)]P_{in2}, \quad (8)$$

where R_{od1} and R_{ev1} are defined as in Eq. (7a), interchanging everywhere with r_1 and r_2. If $r_1 = r_2$, then $R_{ev1} = R_{ev2} = R_{ev}$ and $R_{od1} = R_{od2} = R_{od}$.

Summarizing, a theory of fiber optic radiometry has been formulated. The model is a general one and can be employed to deal with many of the problems encountered in fiber optic radiometry, particularly in IR radiometry. Once the input power distribution $P_{in}(\theta,\gamma,\lambda)$ and the thermal sources have been determined, the problem of radiation guided by the fiber as bounded and tunneling skew rays, and interacting with the guiding medium, can be solved explicitly. In the following sections, we apply this theory to practical cases such as the thermal radiation emissivity of multimode fibers and fiber optic distributed thermal sensors (FDTS). The theory's application to noncontact point thermal sensing by fiber optic radiometry will be discussed in a subsequent paper.

III. Emissivity of Multimode Fibers

To determine fiber emissivity, we examine the total thermal emission from the fiber endfaces compared with the emission of a blackbody whose surface has the same area (πa^2) as the fiber's cross section. As we are concerned only with radiation generated within the fiber, we assume that $P_{in1} = P_{in2} = 0$ and that the temperature T of the fiber is uniform along its length. Let us also assume that the fiber's attenuation coefficient α_t is uniform along the longitudinal coordinate x. Integrating Eqs. (7) and (8) over skewness angle γ gives the angular power distribution across inclination angle θ at both fiber endfaces:

$$P_{out}(\theta,\lambda) = 2\pi a^2 W_{bb\lambda}(T)\cos\theta\sin\theta\epsilon_{out}(\theta,\lambda), \quad (9)$$

where

$$\epsilon_{out}(\theta,\lambda) \equiv \frac{4}{\pi}\int_{\gamma=0}^{\pi/2}(\alpha_{ab}/\alpha_t)[1-\exp(-\alpha_tL)](R_{ev}+R_{od})f(\gamma,\theta)d\gamma. \quad (9a)$$

Comparing Eq. (9) with Eq. (A5), one can deduce that the power distribution at the fiber endfaces differs from that of a blackbody with the same area and temperature by the factor ϵ_{out}. We thus identify this factor as the fiber emissivity and support this conclusion by the fact that Eq. (9a) fulfills the condition $\epsilon_{out} \le 1$. Note that the emissivity might be temperature dependent if the fiber's absorption (α_{ab}) is dependent on temperature. The output power in Eq. (9) is expressed in terms of θ in the core medium. This distribution can equally be represented in terms of θ_1 outside the fiber (assuming $n_1 = n_2$). Using the Jacobian transformation given in Eq. (C3) of Appendix C, for both endfaces we obtain

$$P'_{out}(\theta_1,\lambda) = J_1P_{out}(\theta,\lambda) = 2\pi a^2 W_{bb\lambda}(T)\cos\theta_1\sin\theta_1\epsilon'_{out}(\theta_1,\lambda), \quad (10)$$

where

$$\epsilon'_{out}(\theta_1,\lambda) = (n_1/n_{co})^2\epsilon_{out}(\theta,\lambda). \quad (10a)$$

Inclination angles θ and θ_1 are related to each other by $n_1\sin\theta_1 = n_{co}\sin\theta$. Once again, the power distribution at the fiber endfaces (outside the fiber) differs from that of a blackbody by the emissivity factor ϵ'_{out} given in Eq. (10a). In general, fiber emissivity is spatially and spectrally distributed in a different way from a Lambertian gray emitter but can be tailored through the fiber parameters of the core and the cladding.

Let us examine Eq. (9a) in two simplified cases which describe the basic characteristics of fiber emissivity. In the first example, consider a step idex fiber with uniform core absorption [Eq. (B5)]. The scattering coefficient α_{sc} depends only on inclination angle θ and not on skewness angle γ. We assume that $n_{co} = n_1$ to exclude the effect of successive reflections at the fiber endfaces. This leads to $R_{ev} = 1$ and $R_{od} = 0$, so that Eq. (9a) is reduced to

$$\epsilon_{out}(\theta,\lambda) = \frac{\alpha_{ab}(\theta,\lambda)}{\alpha_t(\theta,\lambda)}\{1-\exp[-\alpha_t(\theta,\lambda)L]\}, \quad \text{for } \theta \le \theta_c,$$
$$\epsilon_{out}(\theta,\lambda) = \frac{\alpha_{ab}}{\alpha_t}[1-\exp(-\alpha_tL)]\frac{4}{\pi}\int_0^{\pi/2}f(\gamma,\theta)d\gamma, \quad \text{for } \theta > \theta_c, \quad (11)$$

where $\alpha_{ab} = \alpha_{co}/\cos\theta$. Equation (11) has a simple interpretation: fiber emissivity is merely the absorption fraction (α_{ab}/α_t) of the fiber's attenuation factor. The scattering fraction does not contribute to fiber emissivity. An illustration of Eq. (11) is shown in Figs. 3(a) and (b).

In the second case we examine fiber emissivity at its

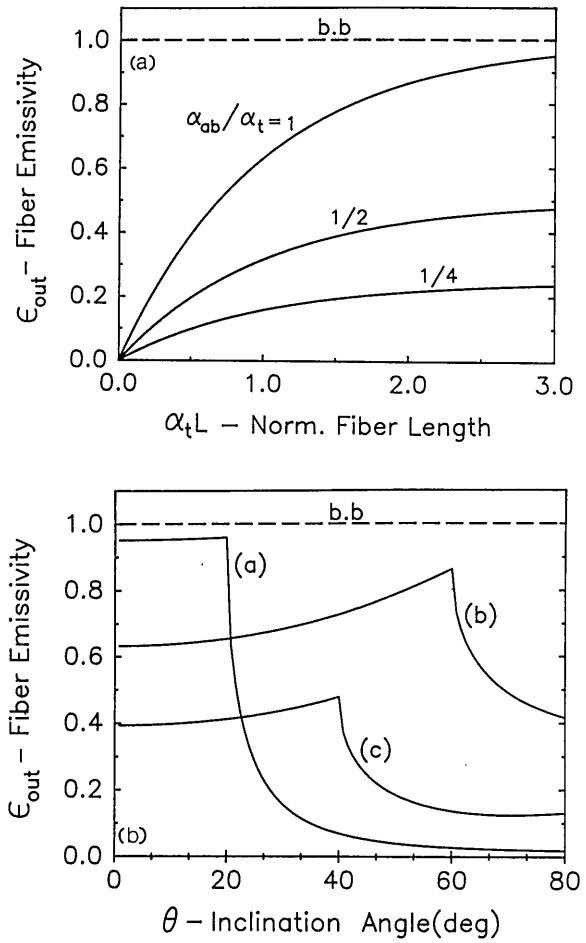

Fig. 3. (a) Fiber emissivity as a function of the fiber's optical length for various absorption fractions, Eq. (11). The dashed line represents a blackbody. (b) Fiber's angular emissivity as a function of the inclination angle for various fiber parameters: (a) $\theta_c = 20°$, $\alpha_{co}L = 3$; (b) $\theta_c = 60°$, $\alpha_{co}L = 1$; (c) $\theta_c = 40°$, $\alpha_{co}L = 0.5$. Scattering loss was ignored ($\alpha_{sc} = 0$).

extreme limit in a highly absorbing fiber with $\alpha_{ab}L \gg 1$ and $\alpha_{sc} \ll \alpha_{ab}$. No radiation can be transmitted between the endfaces, as it is totally absorbed in the fiber. Hence, any radiation emitted from the fiber endfaces has been generated within the fiber, and the emissivity in Eq. (10a) is therefore reduced to

$$\epsilon'_{out}(\theta_1,\lambda) = [1 - r(\theta_1,\lambda)](n_1/n_{co})^2, \quad \text{for } \theta_1 \le \theta_{1c}. \tag{12}$$

We see that even in a totally absorbing fiber emissivity cannot reach unity and is determined by the Fresnel transmission factor for the fiber endfaces and the ratio of the refractive indices of the fiber core and the surrounding medium.

Summarizing, an expression has been derived for the angular emissivity of multimode fibers. This expression might be helpful in various applications of IR fibers. Fiber emissivity [Eq. (10a) or Eq. (11)] was found to be a function of fiber absorption, scattering, the fiber's length, the critical angle, and the core's refractive index. These parameters may be used to tailor a flexible fiber optic thermal radiation source with the advantage that the fiber output endface behaves as a well-defined cold aperture.

IV. Fiber Optic Distributed Thermal Sensors

In this section we employ the formultion of Sec. II to derive a theory for the fiber optic distributed thermal sensor (FDTS).[7] This sensor is a modified fiber optic formed by deliberately inducing a certain absorption profile in a multimode IR fiber. The sensor needs no external radiation source for its operation. When the sensing length of the modified fiber is heated, IR radiation is generated within the fiber and guided through it to the output endfaces. In a first-order sensor, measuring this radiation gives a signal proportional to the average temperature distributed spatially along the length of the fiber. A second-order sensor gives a signal linearly proportional to the location of hot spots along the sensing length. Several fiber absorption profiles are considered in the following theory of the FDTS: The power coupling strength into guided radiation is derived for each profile. A first-order sensor is considered to determine the optical parameters which will yield maximum sensor sensitivity for each absorption profile of the FDTS. The temperature and the spatial resolution of the sensor are also analyzed. Finally, a theory of a second-order sensor is presented.

To gain an insight into the FDTS, let us first examine the way the thermal power generated from each fiber element Δx is spatially distributed across the invariant of ray guiding: inclination angle θ and skewness angle γ. Three basic types of absorption are discussed [see Fig. 5(lower)]. In the first type, the fiber has an absorbing core with a positive profile and nonabsorbing cladding (P profile), and is characterized by

$$\alpha_{co}(r) = \begin{cases} \alpha_{co} & b \le r \le a, \\ 0 & r < b, \end{cases} \quad A_p = (a^2 - b^2)/a^2 \le 1. \tag{13a}$$

Radius b is inside core radius a such that $b \le a$. A_p is the normalized absorbing cross-sectional area, or absorption profile, of the P type. In the second type, the fiber has an absorbing core with a negative profile and nonabsorbing cladding (N profile) and is characterized by

$$\alpha_{co}(r) = \begin{cases} 0 & b \le r \le a, \\ \alpha_{co} & r < b, \end{cases} \quad A_n = b^2/a^2 \le 1, \tag{13b}$$

where A_n is, by analogy, the normalized absorbing cross-sectional area, or absorption profile, of the N type. Any core absorption with a step profile can be considered as a superposition of the P and N profile types. The third profile type discussed is extended absorbing cladding with a nonabsorbing core (E profile) and is characterized by

$$\alpha_{cl}(r) = \begin{cases} \alpha_{cl} & c \ge r \ge a, \\ 0 & r \le a, \end{cases} \quad A_e = \frac{c - a}{\lambda}, \tag{13c}$$

where A_e is the absorption profile of the E type, assumed to be sufficiently high ($A_e > 5$) for the cladding to extend beyond the greatest evanescent penetrating depth.[9]

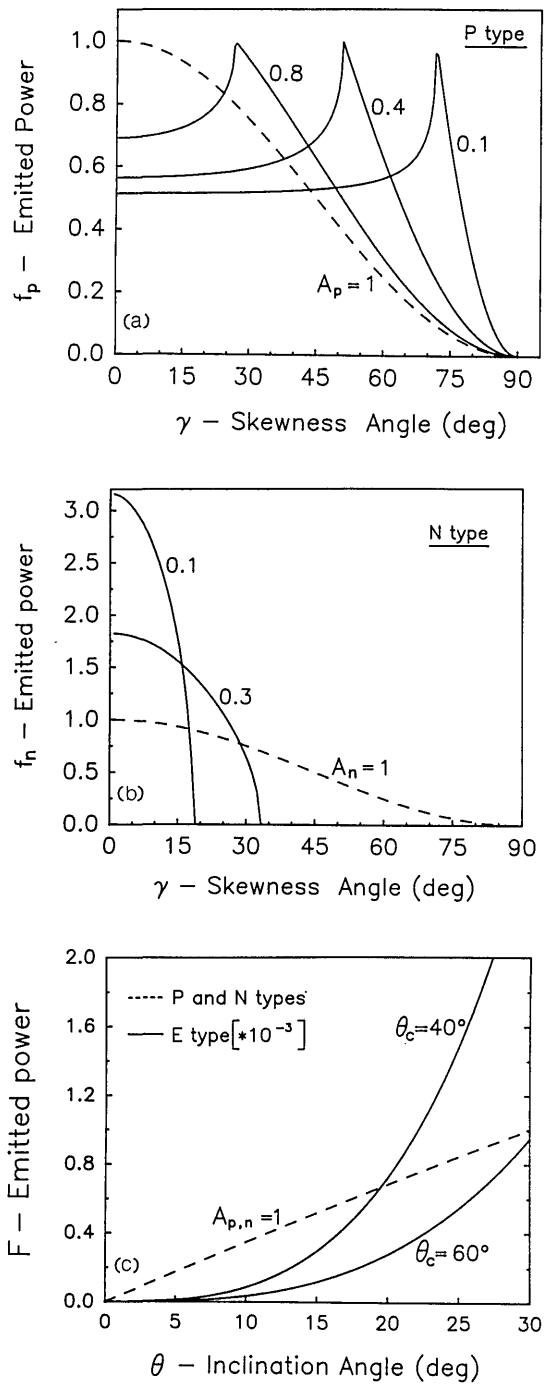

Fig. 4. (a) Skewness distribution of thermal radiation (irrespective of θ) emitted from a fiber element for various absorbent cross-sectional areas A_p of a fiber with a P type profile, Eq. (14a). (b) Same as (a) for various A_n of the N type profile. (c) Angular (θ) distribution of thermal power emitted from fiber elements of the three profile types ($\theta_v = 30°$), Eq. (15a).

The distribution of the power generated from a unit length element of fiber having uniform temperature T is determined by the first term in Eq. (3). Substituting in it the corresponding expression α_{ab}, Eq. (B7) or Eq. (B9), for each of the fiber types [Eq. (13)], we obtain

$$P_{p,n}(\theta,\gamma,\lambda) = \delta_{p,n} W_{bb\lambda}(T)\alpha_{co}\sin\theta f_{p,n}(\gamma,A),$$
$$P_e(\theta,\gamma,\lambda) = \delta_e(\lambda) W_{bb\lambda}(T)\alpha_{cl}\frac{\sin^3\theta}{\sqrt{\sin^2\theta_c - \sin^2\theta}} f_e(\gamma), \tag{14}$$

where

$$\delta_p = 8(a^2 - b^2), \quad \delta_n = 8b^2, \quad \delta_e = \frac{8a\lambda}{2\pi n_{cl}^r \sin^2\theta_c},$$

and where f_p, f_n, and f_e are the skewness distribution functions for the three fiber types given as follows:

$$f_e(\gamma) = \frac{(\sin^2\theta_c - \sin^2\theta)^{1/2}\cos^2\gamma}{(\sin^2\theta_c - \sin^2\theta\cos^2\gamma)^{1/2}}, \quad \text{for } \theta < \theta_c,$$
$$f_{p,n}(\gamma,A) = \cos\theta\cos^2\gamma\rho_{p,n}(\theta,\gamma,A)/A_{p,n}, \quad \text{for } \theta < \theta_c, \tag{14a}$$

where $\rho_{p,n}$ is the fiber's effective absorption coefficient α_{ab} for the P and N profiles, respectively, normalized by the bulk absorption coefficient of the core. Substituting Eqs. (13a) and (13b) into Eq. (B7) gives ρ_p and ρ_n explicitly:

$$\rho_p \equiv \frac{\alpha_{ab}}{\alpha_{co}} = \frac{1}{\cos\theta}\begin{cases} 1, & \sin\gamma \geq \sqrt{1 - A_p}, \\ 1 - (1 - A_p - \sin^2\gamma)^{1/2}/\cos\gamma & \sin\gamma \leq \sqrt{1 - A_p}, \end{cases}$$

$$\rho_n \equiv \frac{\alpha_{ab}}{\alpha_{co}} = \frac{1}{\cos\theta}\begin{cases} 0, & \sin\gamma \geq \sqrt{A_n}, \\ (A_n - \sin^2\gamma)^{1/2}/\cos\gamma, & \sin\gamma \leq \sqrt{A_n}. \end{cases} \tag{14b}$$

The skewness function $f_p(f_n)$ in Eq. (14) is illustrated in Figs. 4(a) and (b). It describes, for various $A_p(A_n)$ with the same α_{co}, the way in which the power emitted from the element into each inclination angle θ is distributed across skewness angle γ. It is apparent, particularly for low absorption profiles, that the absorbing core of the P type profile radiates power mostly into high skew angles (helical rays), while the absorbing core of the N type profile radiates mostly into skew angles (almost meridional rays). The skewness distribution f_e of a fiber with extended absorbing cladding is to a good approximation independent of θ and coincides with the $f_{p,n}$ of a uniformly absorbing core with $A_{p,n} = 1$ [see Figs. 4(a) and (b)]. The power distribution across inclination angle θ of the radiation emitted from a unit length element of fiber is obtained by integrating Eq. (14) over the whole γ range. Accordingly,

$$P_{p,n}(\theta,\lambda) = \pi a^2 W_{bb\lambda}(T)\alpha_{co}F_{p,n}(\theta),$$
$$P_e(\theta,\lambda) = \pi a^2 W_{bb\lambda}(T)\alpha_{cl}F_e(\theta,\lambda). \tag{15}$$

F_p, F_n, and F_e are the inclination distribution functions for the three profile types given as follows:

$$F_{p,n}(\theta) = 2A_{p,n}\sin\theta,$$
$$F_e(\theta,\lambda) = \frac{4\lambda}{\pi^2 a n_{cl}^r \sin^2\theta_c}\sin^3\theta\int_0^{\pi/2}\frac{\cos^2\gamma}{\sqrt{\sin^2\theta_c - \sin^2\theta\cos^2\gamma}}d\gamma. \tag{15a}$$

Equation (15a) is illustrated in Fig. 4(c). As can be seen, the power inclination distributions F_p and F_n (for P and N type profiles) are identical, in spite of the

difference between the power skewness distributions f_p and f_n. It would appear that the higher the mode θ, the more power is coupled into it. Higher modes are heavily populated, particularly in a fiber with extended absorbing cladding (E type). Here the relative mode population increases according to the third power of the mode number (θ), while in the P and N types it increases only according to the first power. This can be explained by considering the interaction mechanism. The higher the mode up to critical angle θ_c, the greater will be the penetration depth of the evanescent field in the cladding and thus the stronger the interaction between the guided mode and the absorbing–emitting cladding. This mechanism, which is wavelength dependent, determines the coupling strength between the thermal radiation of the cladding and the guided modes.

An important result of this formulation is that we are now able to determine which of the two types, core absorption or cladding absorption, can couple more thermal power into the guided modes. The total power coupled in each profile type is obtained by integrating Eq. (15) for θ up to θ_v (the field of view over which the radiation is measured). The coupling strength ratio (CSR) for the two fiber types is thus given by

$$\mathrm{CSR} = \alpha_{co} \int_0^{\theta_v} F_{p,n} d\theta \Big/ \alpha_{cl} \int_0^{\theta_v} F_e d\theta. \tag{16}$$

In IR silver halide fibers,[10] for example, the typical specifications, $\lambda = 8\,\mu\mathrm{m}$, $a = 400\,\mu\mathrm{m}$, $n_{cl}^r = 1.5$, $\theta_C = 60°$, $\theta_v = 30°$, $\alpha_{co} = \alpha_{cl}$, yield a CSR $\simeq 2 \times 10^3 A_{p,n}$, i.e., the thermal power coupled into the fiber by a uniformly absorbing core ($A_p = 1$) is 3 orders of magnitude greater than that coupled by extended absorbing cladding with the same bulk absorption value. Only cladding with α_{cl} 3 orders of magnitude greater ($\alpha_{cl} \simeq 2 \times 10^3 \alpha_{co}$) gives the same power coupling strength as the absorbing core.

A. First-Order FDTS, Linear Thermal Sensing

In this section we examine the performance of the fiber optic distributed thermal sensor in a linear sensing mode. We consider the three absorbing fiber profiles defined in Eq. (13). It is assumed that only the absorption of a section h of the whole fiber length L is modified (see Fig. 5). This section is the sensing length, while the rest of the fiber is ideally nonabsorbing and serves only as a flexible waveguide transmitting the radiation generated in the sensing region to the measuring device. Let us suppose that a steady state temperature difference $\Delta T(x)$ is created along the fiber's sensing length. By Eq. (7), an output power difference (distributed across θ and γ) is generated at the fiber endface. The output power difference emerging into a given field of view $2\theta_{1v}$ (or equivalently $2\theta_v$ in the core medium) was calculated by integrating the power difference over the whole range of γ and θ and defining a normalizing geometric factor c_g. Accordingly,

$$\Delta P_{\mathrm{out2}}(\theta_v,\lambda) = c_g \frac{1}{h} \int_0^h \Delta W_{bb\lambda}[\Delta T(x)] \xi dx, \tag{17}$$

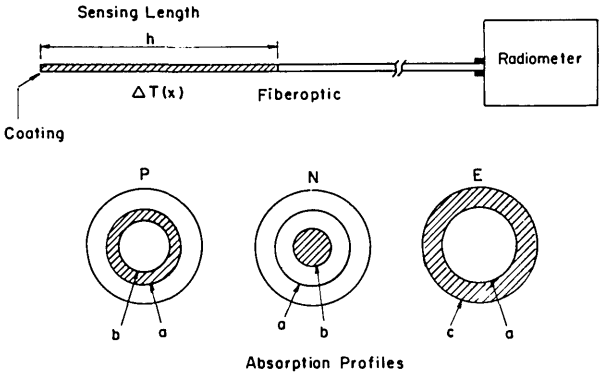

Fig. 5. First-order fiber optic distributed thermal sensor. The three fiber absorption profiles of the sensing section are illustrated.

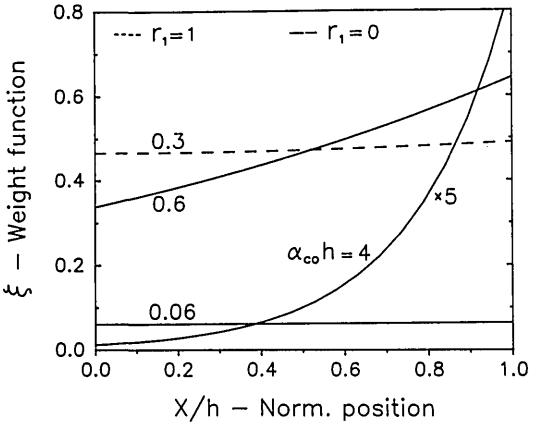

Fig. 6. Weight function of the fiber's sensing elements along the length of the distributed thermal sensor, Eq. (17b) (P type, $A_p = 1, r_2 = 0, \alpha_{sc} = 0$).

where

$$c_g \equiv \pi a^2 \sin^2\theta_v = \pi a^2 (n_1/n_{co})^2 \sin^2\theta_{1v}, \tag{17a}$$

$$\xi = \int_0^{\theta_v} d\theta \int_0^{\pi/2} d\gamma g_s h \alpha_{ab} \{\exp[-\alpha(L)] R_{ev2} \exp[\alpha(x)] + R_{od2} \exp[-\alpha(x)]\}, \tag{17b}$$

and we defined $g_s \equiv g/c_g$. It should be noted that Eq. (17) is valid only as long as

$$\frac{\partial(\alpha_{ab} W_{bb\lambda})}{\partial T} \simeq \alpha_{ab} \frac{\partial W_{bb\lambda}}{\partial T},$$

i.e., the absorption difference due to the difference in temperature is negligible. Equation (17) is interpreted as distributed thermal sensing in a fiber section of length h. This is a spatial averaging of the difference in the blackbody radiation power, $\Delta W_{bb\lambda}(\Delta T)$, emitted from each fiber element along the sensing section, weighted by a position factor $\xi(x)$. The weight function ξ underlies all the physics of the distributed thermal sensor and can be represented as a polynom of the normalized position x/h along the sensing length. The polynom order depends on the product of the sensing length and the fiber's absorption ($h\alpha_{ab}$). By way of an example, Eq. (17b) is illustrated in Fig. 6 for a fiber

with a uniformly absorbing core ($A_p = 1$). Different values of $\alpha_{co}h$ reveal three typical weight functions of the normalized position x. It should be noted that fiber emissivity (as can be deduced from Sec. II) is the zero moment of the weight function given by

$$\epsilon_{out} = \frac{1}{h}\int_0^h \xi dx.$$

In a linear, distributed sensor, all the elements along the fiber's sensing section must be equally weighted, i.e., $\xi(x) = \xi = \text{const}$. This results in a sensor output [Eq. (17)] which is a true average of the thermal power distributed along the fiber's sensing length. The problem is thus converted to an optimization, i.e., determining the fiber parameters which will result in the highest possible ξ, irrespective of position, over the whole sensing length. The factor ξ is identified as the efficiency of the first-order sensor. This can be understood as follows: If ΔT is uniform along the sensing length, by Eq. (17), the output difference $[\Delta P_{out2} = c_g \Delta W_{bb\lambda}(\Delta T)\xi]$ differs from that of a totally absorbing blackbody fiber (with the same geometry, refractive index, and temperature difference) only by the factor ξ. Since sensor emission can never exceed the emission of a blackbody fiber, the value of ξ is thus a measure of the sensor's efficiency, ranging between $0 \le \xi < 1$. Our purpose now is to determine the sensor efficiency of the three fiber profiles: absorbing core with a positive profile (P profile), absorbing core with a negative profile (N profile), and extended absorbing cladding (E profile). This problem was considered in the following ideal condition, giving the highest possible sensitivity: It was assumed that the prominent fiber loss is absorption rather than scattering, i.e., α_{sc} is negligible relative to α_{ab}. In addition, reflections were ignored only at the output endface, $r_2 = 0$, while the input endface was considered once as totally reflecting, $r_1 = 1$, and once as nonreflecting, $r_1 = 0$. In practical terms, this can be achieved by coating the endface on one occasion with a metal reflective coating and on the other with an antireflective coating. Substituting these conditions in Eq. (17b), expanding the exponents to series, and using Eq. (14b), we obtain

$$\begin{aligned} \xi &= 2\xi_0 + 2\xi_2(x/h)^2 + 2\xi_4(x/h)^4 + \ldots, \quad \text{for } r_1 = 1, \\ \xi &= \xi_0 + \xi_1(x/h) + \xi_2(x/h)^2 + \ldots, \quad \text{for } r_1 = 0, \end{aligned} \tag{18}$$

where

$$\xi_i(\alpha h) = (\alpha h)^{i+1}\frac{1}{i!}\int_0^{\theta_v} d\theta \int_0^{\pi/2} d\gamma g_s(\theta,\gamma)[\rho(\theta,\gamma)]^{i+1} \times \exp\{-[\alpha h \rho(\theta,\gamma)]\}, \tag{18a}$$

$$g_s = \frac{8\cos\theta \sin\theta \cos^2\gamma}{\pi \sin^2\theta_v}, \quad \text{for } \theta < \theta_c. \tag{18b}$$

For each absorbing fiber profile there is a value for α and a function ρ to be substituted into Eq. (18a) as follows:

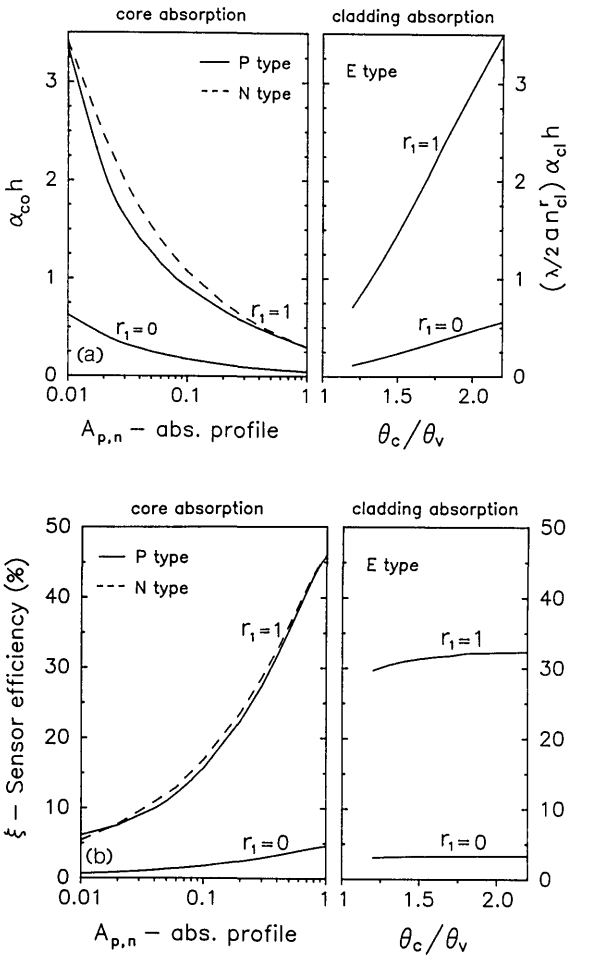

Fig. 7. (a) The αh values ensuring maximum efficiency of the first-order (linear) distributed sensor for the three absorption profiles. The fiber's input endface is considered on one occasion to be totally reflecting ($r_1 = 1$) and on the other to be totally transmitting ($r_1 = 0$), $\theta_v = 30°$. (b) Sensor's efficiency (%) at the optimized αh values of (a).

$$\begin{aligned} &P \text{ profile: } \alpha = \alpha_{co}, \quad \rho = \rho_p(\theta,\gamma,\lambda) \text{ given in Eq. (14b)}, \\ &N \text{ profile: } \alpha = \alpha_{co}, \quad \rho = \rho_n(\theta,\gamma,\lambda) \text{ given in Eq. (14b)}, \\ &E \text{ profile: } \alpha = \frac{\lambda\alpha_{cl}}{2an_{cl}^r}, \quad \rho = \frac{1}{\pi \sin^2\theta_c}\frac{\tan\theta \sin\theta}{\sqrt{\sin^2\theta_c - \sin^2\theta\cos^2\gamma}}. \end{aligned} \tag{18c}$$

The functions ρ represent the relative power absorption across the guiding invariants θ and γ (assuming $\theta_{max} = \theta_v < \theta_c$). From a numerical analysis of the terms in Eq. (18), we deduce that each type of fiber absorption, as defined by the profile factor $A_{p,n,e}$, has a corresponding value $(\alpha h)_A$ which ensures linear, distributed sensing with maximum efficiency $(\xi)_A$. In numerical terms, at this value all the higher terms of Eq. (18) which are dependent on x are negligible relative to the fundamental term ξ_0, yielding a constant ξ with a mean deviation of <2%.

The numerical results of optimization are illustrated in Figs. 7(a) and (b). As can be seen, when the fiber input endface is totally reflecting, $r_1 = 1$, the sensor's efficiency is of an order of magnitude higher than that

of a totally transmitting endface, $r_1 = 0$. Both the P and N profile types demonstrated approximately the same efficiency. The highest sensor efficiency (46%) is achieved when the absorption profile is that of a homogeneously absorbing core $A_{p,n} = 1$ with $r_1 = 1$. However, even if the absorption profile of the core is reduced by 2 orders of magnitude, $A_{p,n} = 0.01$, with optimum absorption efficiency (6%) only reduced by a factor of 8. It should be noted that the optimized sensor parameters ξ and αh for the P and the N types are weakly dependent on θ_v. Moreover, they are independent of the fiber's critical angle θ_c (bear in mind that $\theta_v < \theta_c$). In contrast, in a fiber with extended absorbing cladding, the E type, the optimum sensor parameter αh is dependent on the value of θ_c relative to θ_v (the field of view by which the sensor's radiation output is measured). The smaller the critical angle θ_c, becomes as it approaches θ_v, the higher will be the fiber's absorption [see Fig. 4(c)] and thus the lower the optimum αh value of the sensor. This is a consequence of the evanescent field's penetrating deeper into the cladding as the mode nears cutoff. However, the optimum efficiency of the E type sensor (32%) is only slightly dependent on θ_c and is of the same order as that of the P and N type sensors. It should be noted that this efficiency is achieved with a much higher bulk absorption value for the cladding.

An example with typical values is now described, based on Fig. 7. For any given absorption profile type there is an optimal αh. Hence, selecting the value h of the desired sensing length determines the value of α which will maximize the sensor's efficiency. To obtain a linear sensing length of $h \simeq 30$ cm, the bulk absorption of the core [$\alpha_{co} = (\alpha h)/h$] should be (with $A_{p,n} = 1$, $r_1 = 1$) $\alpha_{co} \simeq 10^{-2}$ cm^{-1}. To obtain the same linear sensing length with a profile of extended absorbing cladding, the bulk absorption of the cladding [$\alpha_{cl} = (\alpha h) n_{cl}^r 2a/\lambda h$] should be (with $a = 400\ \mu$m, $n_{cl}^r = 1.5$, $\lambda = 8\ \mu$m, $\theta_c = 60°$, $\theta_v = 30°$, and $r_1 = 1$) $\alpha_{cl} \simeq 15$ cm^{-1}, i.e., higher by 3 orders of magnitude than the bulk absorption of the core. Such a sensor can be created by coating current state-of-the-art IR bare fiber cores with IR absorbing materials. In all absorption profiles, the greater the sensing length, the lower the bulk absorption which will ensure maximum efficiency. However, the minimum value for bulk absorption (determining the maximum linear sensing length) is limited by the assumption already made, that the losses in the fiber are due much more to absorption than to scattering ($\alpha_{ab} \gg \alpha_{sc}$). Otherwise the sensor's efficiency will be reduced to values lower than those in Fig. 7. This requirement also makes this model of the FDTS valid for imperfect fibers, since mode spreading due to scattering is insignificant within sensing length h, where absorption losses are prominent.

The various absorption profiles have so far been considered from the point of view of optics. A thermodynamics discussion is beyond the scope of this paper. However, basic principles should be considered. The response time and the thermal disturbance of the distributed sensor should be kept to a minimum. This can be achieved by core and cladding materials having a low specific heat as well as low thermal conductivity. Fortunately, the dielectric materials of IR fibers are able to meet these requirements. The absorption profile of the FDTS also plays an important role in the challenge of reducing the time response of the sensor. For example, in thermal sensing by convection or conduction with the FDTS, the response time of an E type profile, with a thin absorbing coating as cladding, will be much shorter than that of a very high P type profile ($A_p \simeq 1$), since heat diffusion into the active sensing layer takes less time to reach a steady state in the cladding than it does in the core. On the other hand, thermal sensing by radiation (penetrating the core–cladding interface and being absorbed in the fiber) is preferable with a low N type profile. This profile is less sensitive to thermal fluctuation in the outer shell of the fiber caused by convection of the surrounding air. In conclusion, both optical and thermal properties should be considered in profile design for each application of the distributed sensor.

In a practical case, the radiation output from the sensor is measured within a spectral detection range between λ_a and λ_b, rather than at one wavelength. In that case, the total power difference output of the sensor can be obtained by integrating Eq. (17) over λ:

$$\Delta P_{\text{out}} = c_g \frac{1}{h} \int_0^h \Delta W_{\lambda_a - \lambda_b}[\Delta T(x)]dx, \tag{19}$$

where

$$\Delta W_{\lambda_a - \lambda_b} = \int_{\lambda_a}^{\lambda_b} \xi_A(\lambda) \Delta W_{bb\lambda}(\Delta T) d\lambda. \tag{19a}$$

As can be seen, the linear form of distributed sensing thermal radiation remains as it was in Eq. (17). Moreover, Eq. (19) can represent, within a certain range, a distributed linear sensing of temperature rather than thermal radiation. The range in which this can be done is specified by the properties of Planck distribution as follows: For each temperature T_0 and spectral detection window $\lambda_a - \lambda_b$, there is a maximum temperature range $\Delta T_{\max}$ centered at T_0 in which $\Delta W_{\lambda_a - \lambda_b}$ approximated well to linear dependence on ΔT (see Fig. 8). For example, around any temperature higher than 300 K and in the 5–15 μm spectral range with $\xi_A =$ constant, ΔW_{5-15} is linearly proportional to ΔT (with a mean deviation of <2%) within a temperature range >50 K. Within these limits, Eq. (19) can be rewritten as

$$\Delta P_{\text{out}} = K \frac{1}{h} \int_0^h \Delta T(x) dx, \tag{20}$$

where

$$K = c_g \int_{\lambda_a}^{\lambda_b} \xi_A(\lambda) \beta_{bb\lambda}(T_0) d\lambda, \tag{20a}$$

$$\beta_{bb\lambda}(T_0) \equiv c_1 c_2 / \lambda^6 T_0^2 [\exp(c_2/\lambda T_0) - 1][1 - \exp(-c_2/\lambda T_0)]. \tag{20b}$$

Constants c_1 and c_2 have already been given in Eq. (1a). By measuring the radiation at one point in the fiber output, one can determine the average temperature

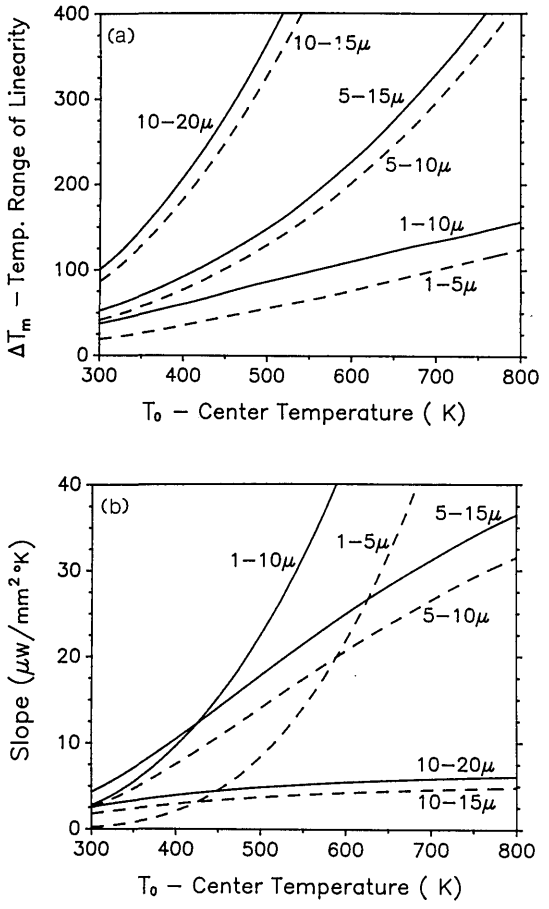

Fig. 8. (a) Maximum temperature range ΔT_{max}, centered around T_0, which yields linear dependence of blackbody power on temperature difference ΔT for various spectral windows. The mean temperature deviation of the real curve from a linear fitting ($\langle \Delta T_{dev} \rangle / \Delta T_{max}$) is <2%. (b) Slope representing the linear dependence of blackbody power on temperature (at the ΔT_{max} range) as a function of the center temperature T_0 for various spectral windows. The steeper the slope, the higher the temperature resolution of the thermal sensing.

distributed along the fiber's sensing length. In other words, the FDTS senses $\Delta T \Delta x$ linearly, rather than ΔT alone as in ordinary point thermal sensors. Introducing the fiber's sensing length into a region with a temperature difference ΔT_i along the fiber path Δx_i gives

$$\Delta P_{out} = K \frac{1}{h} \sum_i \Delta T_i \Delta x_i.$$

Constant K of Eq. (20a) (proportional to $\xi a^2 \sin^2\theta_v$) determines the sensitivity of this sensor. It increases linearly with efficiency ξ, and with the square of the fiber's radius and the field of view ($\sin^2\theta_v$). Sensitivity K is maximized when the spectral detection range from λ_a to λ_b is centered around the wavelength of maximum $\beta_{bb\lambda}(T_0)$. According to Eq. (20b), the wavelength of the maximum is given by $\lambda_{max} T_0 = 2404\ \mu$K, i.e., 8 μm at 300 K. Thus, IR fibers are best suited for distributed thermal sensing.

Our concern now is to determine the temperature and spatial resolution of the linear, distributed sensor. Consider a device measuring the radiation emitted from the fiber's output endface. There is a minimum power difference $\Delta P_{out}^{(min)}$ which the device can resolve from the noise. This power difference corresponds to the minimum temperature difference created along a section Δx which can be detected by the measuring device. Using Eq. (20), this minimum resolvable temperature difference (MRΔT) is given by

$$\mathrm{MR}\Delta T = [\Delta P_{out}^{(min)}/K] \frac{h}{\Delta x}. \tag{21}$$

It is helpful to represent Eq. (21) in terms of the minimum temperature difference $\Delta T_{bb}^{(min)}$, resolvable by the same measuring device, from a blackbody surface with the same geometry as the fiber's endface. Using Eq. (20a), Eq. (21) can be replaced by

$$\mathrm{MR}\Delta T = \left[\Delta T_{bb}^{(min)} \frac{n_{co}^2}{\xi_A} \right] \frac{h}{\Delta x}, \tag{22}$$

where we have assumed that the sensor's efficiency ξ_A is constant over the spectral detection range from λ_a to λ_b. As a representative example, consider $\Delta T_{bb}^{(min)} \simeq 0.01$ K, $n_{co} = 2$, and $\xi_A \simeq 0.4$. If a temperature difference is created along only one-tenth of the whole fiber's sensing length, this temperature must exceed 1 K to be detected. By analogy to Eq. (22), we also derive the minimum resolvable normalized length $\Delta x_{min}/h$. This ratio is interpreted as the minimum normalized length over which a given temperature difference of ΔT can be detected. Accordingly,

$$\mathrm{MR}\left(\frac{\Delta x}{h}\right) = \left[\Delta T_{bb}^{(min)} \frac{n_{co}^2}{\xi_A} \right] \frac{1}{\Delta T}. \tag{23}$$

Equation (23) defines the spatial resolution of the distributed sensor. An interesting point about this sensor is the independence of $\Delta x_{min}/h$ and h the absolute length of the sensor. This emphasizes the possibility of using short sensing lengths without reducing the spatial resolution. Finally, we note that such a sensor can also have a sensing length which is discontinuously extended over discrete sensing regions, interconnected by nonmodified transparent fiber sections.

B. Second-Order FDTS, Location Sensing of Hot Spots

A theoretical analysis is now presented of a second-order fiber optic distributed thermal sensor. Such a sensor is used to detect the position of local overheating or a hot spot along the sensing length of the fiber. The configuration of this thermal sensor is illustrated in Fig. 9. Sensing section h of the fiber is formed by inducing deliberate core or cladding absorption in this part of the fiber. The location signal is obtained by processing the power output signals from both fiber endfaces. This sensor is being considered in ideal conditions which give the highest sensitivity. It is assumed, as in the case of the first-order sensor, that absorption is the main cause of power loss in the sensing region. Out with this region, losses are negligible. Both fiber endfaces are coated with an antireflective

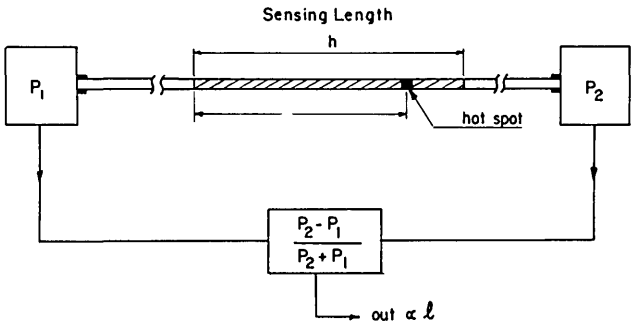

Fig. 9. Second-order fiber optic distributed thermal sensor. A configuration for linear sensing of location l of a hot spot.

coating ($r_1 = r_2 = 0$). Let us suppose that at position l, a local temperature difference $\Delta T(x')$ is created in the fiber due to overheating. Using Eq. (7), we obtain [by analogy to Eq. (17)] the power difference output from endface 2:

$$\Delta P_{out2}(\theta_v,\lambda) = c_g \frac{1}{h}\int_{-\tilde{x}}^{+\tilde{x}} \xi \Delta W_{bb\lambda}[\Delta T(x')]dx', \tag{24a}$$

where $\tilde{x}$ is the extended region of overheating, measured on a coordinate system x' centered at location point l. The weighting factor ξ is expressed as follows:

$$\xi = \xi_0 + \xi_1(l + x')/h + \xi_2[(l + x')/h]^2 + \ldots. \tag{24b}$$

The constants ξ_i are defined as in Eqs. (18a) and 18c). To obtain uniform sensitivity of the overheating location l in the whole sensing section, we require linear dependence of ΔP_{out} on l (a second-order FDTS). The problem is again converted to an optimization, i.e., determining the fiber parameters leading to ξ dependence of the form $\xi = I + S(l + x')/h$, where I and S are, respectively, the intercept and the slope of a linear regression fitted to ξ. From a numerical analysis of ξ in Eq. (24a), we deduce that for each absorption profile of type $A_{p,n,e}$ there is a corresponding value $(\alpha h)_A$ which ensures a linear fit with ξ and a maximum slope (the mean deviation of the fit is <2%). The optimized αh values obtained for a second-order FDTS are 1 order of magnitude greater than those obtained for the first-order sensor [Fig. 7(a)]. Thus, given absorption profile A and the sensing length h required, we obtain a value for α [defined in Eq. (18c)] which will ensure the highest sensitivity for the second-order FDTS. With this optimization, Eq. (24) can be rewritten as

$$\Delta P_{out2} = \left(I + S\frac{l}{h}\right)c_g \frac{1}{h}\int_{-\tilde{x}}^{+\tilde{x}} \Delta W_{bb\lambda}[\Delta T(x')]dx', \tag{24c}$$

where the term $(x'/h)S$ has been neglected. This is justified on two grounds. First, the heated region in the fiber is assumed to be much smaller than the whole sensing section ($x' \le \tilde{x} \ll h$). Second, if the temperature difference $\Delta T(x')$ is created symmetrically around l (an even function), this term vanishes when an odd function is integrated over x'. Although ΔP_{out} in Eq. (24b) is a linear function of heat location l, we still require information on temperature $\Delta T(x')$ to determine the location of l. To avoid this, we also use the information available from endface 1. Using Eq. (8), we obtain the difference in output power from endface 1:

$$\Delta P_{out1} = \left(I + S - S\frac{l}{h}\right)c_g \frac{1}{h}\int_{-\tilde{x}}^{+\tilde{x}} \Delta W_{bb\lambda}[\Delta T(x')]dx'. \tag{25}$$

Both outputs from the fiber are thus related to each other by $\Delta P_{out1}(l) = \Delta P_{out2}(h - l)$. Generating a signal ratio (SR) between the difference in the outputs and their sum gives

$$\mathrm{SR} \equiv \frac{\Delta P_{out2} - \Delta P_{out1}}{\Delta P_{out2} + \Delta P_{out1}} = B\left(\frac{l}{h} - \frac{1}{2}\right), \tag{26}$$

where $B \equiv 2S/(2I + S)$. This signal is linearly dependent on the normalized location l/h and requires no further information on the temperature to determine the location. The slope of the SR dependence on l/h is twice as steep as the signal from a single output. Using both expressions, that of Eq. (26) and that obtained from the sum of Eqs. (24b) and (25), it is possible to determine the location and the average temperature of the hot spot. Proportionality constant B is determined by the optimization values of I and S. The greater B, the higher will be the sensor's resolution.

Summarizing, a theory has been presented of the fiber optic distributed thermal sensor. The sensor is based on the self-generation of guided thermal radiation in the fiber due to absorption. Three profiles of fiber absorption have been discussed: surface core, bulk core, and cladding absorption [Eq. (13)]. The P type absorption profile radiates power guided in the fiber mostly in high skew angles by helical rays, while the N profile radiates power in low skew angles guided by nearly meridional rays. The guided radiation coupled by the P, the N, and particularly the E type profiles heavily populate modes with high inclination angle up to cutoff (Fig. 4). The coupling strength of guided thermal radiation by extended absorbing cladding is 3 orders of magnitude less than that of an absorbing core with the same bulk absorption. However, cladding with an absorption coefficient 3 orders of magnitude greater yields the same coupling strength as the absorbing core.

The position weight function, describing the relative sensitivity of each fiber element along the length of the distributed sensor, is dependent on the profile of absorption (Fig. 6). For each profile and sensor length there is a corresponding optimum bulk absorption coefficient ensuring distributed linear sensing with a uniform weight function irrespective of position, i.e., a first-order sensor (Fig. 7). With such a sensor, it is possible to detect average spatial temperature distribution along its path. The sensitivity of the FDTS depends on the fiber's diameter, critical angle, field of view, and the sensor's efficiency. The efficiency of a fiber sensor having one endface coated with a reflective coating is as high as 46% relative to a blackbody. A second-order sensor can be created by a bulk absorption coefficient 1 order of magnitude higher. A sensor of this kind may be used to detect hot spots along the sensing length.

C. Discussion

The FDTS is based on core or cladding absorption as a source of thermal radiation guided in the fiber. The optimized absorption values derived for each profile of the FDTS [Fig. 7(a)] may serve as a guide in producing an FDTS of a given sensing length. Several techniques are available for inducing absorption in IR fibers. One is to increase the concentration of impurities with the desired profile in the preform from which the fiber is pulled or extruded. Another is to diffuse impurities into the fiber core, enhancing the surface absorption of the core to obtain a P type FDTS. In silver halide fibers this may also be achieved by exposing the fiber to UV light.[11] An E type profile may be obtained by simply coating a bare fiber core with an IR absorbing material as cladding. The cladding absorption required to produce an FDTS is much higher than the core absorption required to produce an FDTS of the same sensing length. In this paper only extended absorbing cladding has been considered. However, an FDTS can also be produced by coating the bare fiber core with a thin absorbing film ($c - a \ll 5\lambda$). An optimization of this sensor can be derived by the same formulation, and only the expression for fiber modal absorption, Eq. (B9), must be replaced with a corresponding one.[12] Here, film thickness as well as its absorption determines the sensing length of the FDTS. The thinner the film, the higher will be the absorption required to produce an FDTS of the same sensing length.

It should be noted that when inducing nonuniform absorption in the core of a step index fiber, the real refractive index of the core cannot always be considered as uniform. According to Kramers-Kronig relations, the real refractive index can become highly graded, and another formulation must be used. To retain an intuitive picture, the formulation in this paper is intended ideally for step index fibers with a step absorption profile (see Appendix B). However, application of the theory to graded-index fibers is straightforward, if the guiding invariant parameters θ and γ are interchanged with those of the graded index.[13] The optimized sensor parameters will then also depend on the profile of the real refractive index of the fiber, but the basic picture developed in this paper will remain the same. Finally, we expect the distributed thermal sensing effect discussed here to appear in all waveguide types, including hollow fibers.

Appendix A: Blackbody Power Emitted from a Fiber Element

Consider a blackbody fiber element located at a distance x from the endface 1 of the fiber (see Fig. 1). The element's surface area (πa^2) is also the area of the fiber's cross section. Using radiometric theory, we derive the thermal radiation power emitted from the surface of the element into a hemispherical solid angle:

$$P_{bb\lambda}[T(x)] = \int_0^{\pi/2} d\theta 4 \int_0^{\pi/2} d\phi \int_0^a r dr \int_0^{2\pi} d\Phi \times \frac{W_{bb\lambda}[T(x)]}{\pi} \cos\theta \sin\theta \left[\frac{W}{\mu}\right]. \quad \text{(A1)}$$

The factor $rdrd\Phi$ is a differential area on the cross section of the fiber, while $\sin\theta d\theta d\phi$ is a differential solid angle. The rays emitted from each differential area on the element's surface into the same inclination angle θ are guided within the fiber at various skewness angles γ. Angle γ of the ray is determined by the location of the differential area from which the ray emerges and azimuthal angle ϕ of the ray as follows:

$$\sin\gamma = r \sin\phi / a. \quad \text{(A2)}$$

Using Eq. (A2), we represent Eq. (A1) in terms of γ by transforming the variables with corresponding integration limits:

$$P_{bb\lambda}[T(x)] = \int_0^{\pi/2} d\theta \int_0^{\pi/2} d\gamma \int_{a\sin\gamma}^a dr 8 W_{bb\lambda}[T(x)] \times \cos\theta \sin\theta \frac{ra\cos\gamma}{(r^2 - a^2\sin^2\gamma)^{1/2}}. \quad \text{(A3)}$$

Only part of the total power emitted from the fiber element, $P_{bb\lambda}[T(x)]$, is guided in the fiber. The guided part is obtained by introducing a Θ function, which serves as a ray guiding criterion for bounded and tunneling rays, but excludes all refracted rays:

$$\Theta\left(\frac{\sin\theta_c}{\sin\theta} - \cos\gamma\right) = \begin{cases} 1 & \cos\gamma \sin\theta \le \sin\theta_c, \\ 0 & \cos\gamma \sin\theta > \sin\theta_c, \end{cases} \quad \text{(A4)}$$

where θ_c is the critical angle (in the core medium) of meridional rays ($\gamma = 0$), given up $\theta_c = \cos^{-1}(n_{cl}/n_{co})$; n_{co} and n_{cl} are the refractive indices of the core and the cladding, respectively. Incorporating the guiding criterion, Eq. (A4), into Eq. (A3), and evaluating the integral over r gives the guided part of the radiation power generated from the fiber element in terms of guiding invariants θ and γ:

$$P_{bb\lambda}[T(x)] = 8a^2 W_{bb\lambda}[T(x)] \int_0^{\pi/2} \int_0^{\pi/2} \times \cos\theta \sin\theta f(\gamma,\theta) d\gamma d\theta \, [W/\mu], \quad \text{(A5)}$$

where the skewness distribution function is defined as

$$f(\gamma,\theta) \equiv \cos^2\gamma \Theta\left(\frac{\sin\theta_c}{\sin\theta} - \cos\gamma\right). \quad \text{(A5a)}$$

For any inclination angle $\theta \le \theta_c$, $f(\gamma,\theta)$ is reduced to $\cos^2\gamma$. Equation (A5) has an important interpretation: the power emitted from each fiber element is distributed across guiding angles θ and γ irrespective of the fiber's transverse parameters. The problem of radiation generation in the fiber is thus reduced to longitudinal consideration, since angles θ and γ are invariant parameters of the ray's path in the fiber.

Appendix B: Fiber Attenuation Coefficients α_{ab} and α_{sc}

1. Effective Absorption of the Core

The effective absorption coefficient per unit length of fiber is formulated for a core nonuniformly absorbing. Core absorption is defined by ascribing an imaginary component to the refractive index:

$$n_{co}(x,r) = n^r_{co} - i n^i_{co}(x,r), \quad n^i_{co}(x,r) = \frac{\lambda}{4\pi} \alpha_{co}(x,r). \quad \text{(B1)}$$

The superscripts r and i denote real and imaginary parts, λ is the free-space wavelength, and α_{co} is the bulk absorption coefficient of the core. Let us consider only fibers with circular symmetry, such that α_{co} is a function of the cylindrical polar radius r and the longitudinal position x. Although this paper considers only step index fibers, an analysis of Fresnel reflection factors shows that for slight absorption ($n^i \ll n^r$), the nonhomogeneity of n^i_{co} affects neither the trajectories of the guided rays (compared to those of a step index fiber) nor the reflection factors at the fiber's endface. The parameters of the ray's path, inclination angle θ, and skewness angle γ are still invariants, and only nonhomogeneous absorption is introduced along the ray's path. Even if core absorption reaches a level as high as $\alpha_{co} = 1\ \text{cm}^{-1}$ (i.e., 500 dB/m) in any place, we obtain $n^i \simeq 10^{-4} \ll n^r$ for $\lambda < 15\ \mu\text{m}$. This still agrees with the definition of slight absorption and validates the formulation of the step index fiber. The effective absorption coefficient per unit length along the fiber's axis is formulated by calculating the absorption between two successive reflections along the ray's path, multiplied by the number of reflections ν in a unit length of fiber. Accordingly,

$$\alpha_{ab} = \nu \int \alpha_{co}(r)ds, \quad \nu = \frac{\tan\theta}{2a\cos\gamma}, \tag{B2}$$

where the integrand is evaluated along the ray's path between two successive reflections from the core–cladding interface. It is assumed that $\alpha_{co}(r)$ does not vary along the x-axis by a distance much greater than $1/\nu$. The circular symmetry enables us to express ray path s in terms of transverse radius r as follows:

$$s = \frac{a\sin\gamma - (r^2 - a^2\sin\gamma)^{1/2}}{\sin\theta}, \tag{B3}$$

The numerator is simply the projection of the ray's path on the cross section of the fiber. Transformation of the variables in Eq. (B2) using Eq. (B3) gives an explicit expression of α_{ab} in terms of guiding invariants θ and γ. Thus

$$\alpha_{ab}(\theta,\gamma) = \frac{1}{a\cos\gamma\cos\theta}\int_{a\sin\gamma}^{a} \frac{\alpha_{co}(r)r}{(r^2 - a^2\sin^2\gamma)^{1/2}}\,dr. \tag{B4}$$

If the core is uniformly absorbing [$\alpha_{co}(r) = \alpha_{co}$], Eq. (B4) is reduced to

$$\alpha_{ab}(\theta) = \alpha_{co}/\cos\theta, \tag{B5}$$

that is, the effective absorption is independent of skewness angle γ of the ray.

The other case discussed is a double step distribution of bulk absorption along the transverse coordinate r, given by

$$\alpha_{co}(r) = \begin{cases} \alpha_{co}^{(a)} & b \le r \le a, \\ \alpha_{co}^{(b)} & r < b, \end{cases} \tag{B6}$$

where b is a radius within the radius of the core ($b < a$). Substituting this absorption profile into Eq. (B4) gives

$$\alpha_{ab}(\theta,\gamma) = \frac{1}{\cos\theta}\begin{cases} \alpha_{co}^{(a)} & \sin\gamma \ge b/a, \\ \alpha_{co}^{(a)}[1 - \Gamma(\gamma)] + \alpha_{co}^{(b)}\Gamma(\gamma) & \sin\gamma \le b/a, \end{cases} \tag{B7}$$

where

$$\Gamma(\gamma) \equiv \frac{(b^2/a^a - \sin^2\gamma)^{1/2}}{\cos\gamma}.$$

In an ideally distributed sensor, absorption is induced in a highly transparent substrate core. Two extreme cases of core absorption are then discussed, either $\alpha_{co}^{(b)} \ll \alpha_{co}^{(a)}$ or $\alpha_{co}^{(a)} \ll \alpha_{co}^{(b)}$.

2. Effective Absorption of the Cladding

Cladding absorption is a mechanism of power loss resulting from the interaction of evanescent waves of guided modes with absorbing cladding. The expression for this power loss in the ray picture is identical to the Fresnel transmission factor at each turning point on the core–cladding interface (assuming a semi-infinite cladding with $\lambda \ll a$). Thus, the imaginary component of the refractive index in absorbing cladding causes guided rays to be only partially reflected at the turning points. α_{ab} is thus formulated by multiplying Fresnel factor t for the power transmission in each reflection by the number of reflections ν per unit length:

$$\alpha_{ab} = \nu(\theta,\gamma)t(\theta,\gamma,\lambda); \tag{B8}$$

ν has already been defined in Eq. (B2). Fresnel transmission factor t must be calculated for unpolarized radiation. This is justified for two reasons: thermal radiation is unpolarized, and skew rays (which carry most of the thermal power) have an undefined polarization state. Hence, if the cladding absorption is weak ($n^i_{cl} \ll n^r_{co}$) and $\theta < \theta_c$ with θ not too close to θ_c, Eq. (B8) is significantly simplified, and the effective cladding absorption will be well approximated by[13]

$$\alpha_{ab} = \frac{\lambda}{2\pi a}\frac{\sin\theta\tan\theta}{\sin^2\theta_c\sqrt{\sin^2\theta_c - \sin^2\theta\cos^2\gamma}}\left(\frac{\alpha_{cl}}{n^r_{cl}} - \frac{\alpha_{co}}{n^r_{co}}\right). \tag{B9}$$

In cladding with $n^r_{cl} > 1$ and $\lambda < 15\ \mu\text{m}$, Eq. (B9) is valid even if the bulk cladding absorption is as high as $10^2\ \text{cm}^{-1}$ (satisfying $n^i_{cl} \simeq 10^{-2} \ll n^r_{cl}$). Finally, the total effective absorption coefficient of the fiber can be expressed as the sum of the core and cladding absorption: $\alpha_{ab}(\text{fiber}) = \alpha_{ab}(\text{core}) + \alpha_{ab}(\text{clad})$. It should be noted that, in general, fiber absorption might also be temperature dependent.

3. Scattering Losses

One mechanism of power loss due to scattering is the radiation of power out of the fiber by leaking rays, i.e., guided rays with $\theta > \theta_c$ obeying Eq. (A4). These are tunneling skew rays which, despite the planar geometric prediction that they be trapped by total internal reflection, are in fact attenuated due to the curvature of the core–cladding interface in circular fibers. The radiation attenuation coefficient for leaky rays α_{le} can be found elsewhere.[13] However, in multimode short fibers ($V \gg 1, L < 50\ \text{m}$) suited for thermal radiometry,

α_{le} is negligible. Another mechanism causing radiation of power is Rayleigh scattering. If imperfections in the fiber cause diffraction-limited scattering,[14] power coupling between modes becomes significant and the formulation presented here is no longer valid. All radiation losses are represented in this study by the fiber's scattering attenuation coefficient $\alpha_{sc}(\theta,\gamma,\lambda)$.

Appendix C: Inside–Outside Transformation of Power Distribution at the Endfaces

The power output distributions in Eqs. (7) and (8) are expressed in terms of invariant angles θ and γ (in the core medium). The representation of these distributions in terms of equivalent angles $\theta_{1,2}$ and γ (outside the fiber) is derived by a Jacobian transformation. Since skewness angle γ of the ray remains unchanged when it crosses the endfaces (as deduced by Snell's law), the transformation of power is expressed by

$$P_{\text{out1}}(\theta,\gamma)d\theta = P'_{\text{out1}}(\theta_1,\gamma)d\theta_1,$$
$$P_{\text{out2}}(\theta,\gamma) = P'_{\text{out2}}(\theta_2,\gamma)d\theta_2, \tag{C1}$$

where P'_{out1} and P'_{out2} are the power input and output distributions outside the fiber. Angles θ and $\theta_{1,2}$ are related by Snell's law: $n_{co}\sin\theta = n_1\sin\theta_1 = n_2\sin\theta_2$. Differentiating this relationship gives the Jacobian transformation

$$d\theta = J_{1,2}d\theta_{1,2}, \quad J_{1,2} = \frac{n_{1,2}\cos\theta_{1,2}}{(n_{co}^2 - n_{1,2}^2\sin^2\theta_{1,2})^{1/2}}. \tag{C2}$$

Substituting Eq. (C2) into Eq. (C1) gives the inside–outside transformation of power distribution at the fiber's endfaces:

$$P_{\text{out1}}(\theta,\gamma) = \frac{1}{J_1}P'_{\text{out1}}(\theta_1,\gamma), \quad P_{\text{out2}}(\theta,\gamma) = \frac{1}{J_2}P'_{\text{out2}}(\theta_2,\gamma). \tag{C3}$$

References

1. S. R. Mordon, A. H. Cornil, and J. M. Brunetaud, "Temperature Measurement with Zirconium Fluoride Glass Fiber," Appl. Opt. **26,** 607–609 (1987).
2. A. Zur and A. Katzir, "Infrared Fibers for Low Temperature Radiometric Measurements," Appl. Phys. Lett. **48,** 499–500 (1986).
3. V. G. Artjushenko, V. V. Voitsekhovsky, V. J. Masychev, J. V. Zubov, and V. K. Sysoev, "Fiberoptic Device for Simultaneous Laser Power Transmission and Temperature Measurement of Irradiated Object," Electron. Lett. **20,** 983–984 (1984).
4. L. M. Hobrock and J. D. Sneed, "Radiometric Applications of Infrared Fibers," Proc. Soc. Photo-Opt. Instrum. Eng. **320,** 140–143 (1982).
5. A. Katzir, H. F. Bowman, Y. Asfour, A. Zur, and C. R. Valeri, "Infrared Fibers for Radiometer Thermometry in Hypothermia and Hyperthermia Treatment," IEEE Trans. Biomed. Eng. **BE-6,** 634–637 (1989).
6. E. Sinofsky and M. G. Dumont, "Temperature Measurement Using Silica and Fluoride Based Optical Fibers for Biological Applications," Proc. Soc. Photo-Opt. Instrum. Eng. **907,** 131–136 (1988).
7. A. Zur and A. Katzir, "Fiberoptic Distributed Thermal Sensor," Appl. Phys. Lett. **53,** 2474–2476 (1988).
8. D. Marcuse, "Launching Light into Fiber Cores from Sources Located in the Cladding," IEEE/OSA J. Lightwave Technol. **LT-6,** 1273–1279 (1988).
9. N. J. Harrick, *Internal Reflection Spectroscopy* (Wiley, New York, 1967), p. 30.
10. A. Saar, N. Barkay, F. Moser, I. Schnitzer, and A. Katzir, "Optical and Mechanical Properties of Silver Halide Fibers," Proc. Soc. Photo-Opt. Instrum. Eng. **843,** 98–104 (1987).
11. R. Chen, A. Katzir, A. Levite, F. Moser, and D. Weiss, "Absorption and Luminescence of Silver Halide Optical Fibers," J. Opt. Soc. Am. B **3,** 696–700 (1986).
12. J. Wang, D. Christensen, E. Brynda, J. Andrade, J. Ives, and J. N. Lin, "Sensitivity Analysis of Evanescent Fiber Optic Sensors," Proc. Soc. Photo-Opt. Instrum. Eng. **1067,** 11–19 (1989).
13. A. W. Snyder and J. D. Love, *Optical Waveguide Theory* (Chapman & Hall, London, 1983), Secs. 35-13, 7-3, 2-3.
14. A. Saar and A. Katzir, "Scattering Effects in Crystalline Infrared Fibers," J. Opt. Soc. Am. A **5,** 823–833 (1988).